A combined instantaneous normal mode and time correlation function description of the infrared vibrational spectrum of ambient water

Heather Ahlborn, Xingdong Ji, Brian Space, and Preston B. Moore

Citation: The Journal of Chemical Physics **111**, 10622 (1999); doi: 10.1063/1.480415
View online: http://dx.doi.org/10.1063/1.480415
View Table of Contents: http://scitation.aip.org/content/aip/journal/jcp/111/23?ver=pdfcov
Published by the AIP Publishing

A combined instantaneous normal mode and time correlation function description of the infrared vibrational spectrum of ambient water

Heather Ahlborn, Xingdong Ji, and Brian Space[a)]
Department of Chemistry and Biochemistry, Duquesne University, Pittsburgh, Pennsylvania 15282-1530

Preston B. Moore
Department of Chemistry, University of Pennsylvania, Philadelphia, Pennsylvania 19104-6323

(Received 19 July 1999; accepted 22 September 1999)

A formal connection is made between the vibrational density of states (DOS) of a liquid and its approximation by way of instantaneous normal modes (INMs). This analysis leads to a quantum generalization of the INM method (QINM), and to the possibility of evaluating the classical DOS exactly. Further, INM approximations to spectroscopic quantities (e.g., infrared absorption and Raman scattering) follow in a consistent manner by evaluating the appropriate golden rule expressions for harmonic oscillators, using the INM or QINM DOS in place of the true DOS. INM and QINM methods are then applied along with traditional time correlation function (TCF) methods to analyze the entire infrared (IR) spectrum of ambient water. The INM and TCF approaches are found to offer complimentary information. TCF methods are shown to offer an unexpectedly accurate description of the O–H stretching line shape. Further, the 19-fold enhancement in liquid phase absorption compared to the gas phase is also reproduced. INM and QINM methods are used to analyze the molecular origin of the water spectrum, and prove especially effective in analyzing the broad O–H stretching absorption. Further, it is argued that a motional narrowing picture is qualitatively useful in analyzing INM approximations to spectroscopy. © *1999 American Institute of Physics.* [S0021-9606(99)50947-1]

I. INTRODUCTION

Instantaneous normal mode theory has been successful in describing a number of liquid state properties.[1–7] Further, INM theory is an intuitively appealing and effective approach to modeling condensed phase spectroscopy.[5,8–17] At the center of INM approaches is an harmonic approximation to the true Born–Oppenheimer vibrational density of states (DOS). Here, the INM DOS is formally derived as an approximation to the true DOS, and is generalized to include quantum thermodynamic effects (QINM). The derivation also suggests the possibility of relaxing the harmonic approximation and directly calculating the classical vibrational density of states. Because INM methods provide an approximation to the true DOS, spectroscopic quantities can be calculated in a consistent manner by evaluating the relevant frequency domain golden rule expression for harmonic oscillators. This approach leads to an approximation to the spectrum in the form of a weighted DOS. The weighting factor is calculated as a derivative of the relevant quantity with respect to the INM, e.g., when modeling infrared (IR) spectroscopy the weighting factor is the squared dipole derivative with respect to an INM. It has been argued that motional narrowing effects are a major part of what is left out of this approximation, which does not require dynamical input,[9,13,18,19] and the present results are consistent with that picture. Previously, INM methods have primarily been applied to intermolecular spectroscopy, where the INM weighted DOS is often an excellent description of the actual spectrum (as calculated by time correlation function (TCF) methods or measured experimentally), and motional narrowing is not an issue.[9,10,13] It will be demonstrated that INM methods may also be productively employed to analyze intramolecular line shapes, although intramolecular motions can only be quantitatively described when motional narrowing effects are included.

The spectroscopy of water has been extensively examined experimentally and theoretically by a variety of methods.[20–27] In this paper the entire infrared vibrational spectrum of ambient water is investigated using a combination of instantaneous normal mode (INM and QINM), and TCF methods. The primary focus is on analyzing the intramolecular spectroscopy where both INM and TCF methods are found to work remarkably well in a regime where a quantum mechanical approach would seem more appropriate.[12,28] Water was chosen due to its significance in many natural processes, the importance of quantum thermodynamic effects on its structure,[29] and the current availability of high quality experimental IR spectroscopic data.[21,22,30] TCF and INM methodologies are shown to provide complimentary information, and allow for detailed analysis of spectroscopic signatures. Molecular dynamics simulations are employed using simple water models (SPC,TIP3P)[20] which are supplemented with stretching force fields to generate the configurations used to construct the spectra.[31] It is demonstrated that these simple models capture much of the structure and dynamics essential to describing both the intermo-

[a)]Author to whom correspondence should be addressed. Electronic mail: space@space1.chemistry.duq.edu

lecular and intramolecular spectroscopy. Further, it is found that many body polarization effects need only be included for the purpose of calculating the spectra, i.e., in calculating the system dipole moment, and are not included in performing the dynamics.[9,10,32]

Using INM and TCF methods, it is unambiguously demonstrated that the 200 cm^{-1} bump in the water IR spectrum is a result of collective many body polarization effects, as has been argued previously.[32] Use of different detailed balance factors is shown to have a dramatic effect on the intermolecular and intramolecular spectrum,[33–35] although for INM treatments this is not an issue, and this will be discussed in detail below.

The spectral line shape of the O–H stretching region calculated via TCF is shown to be in excellent agreement with experiment when the O–H stretch is modeled as a Morse oscillator, while harmonic representations give answers which have frequencies which are significantly too high, as has been noted previously.[24] INM methodology is employed to analyze the molecular contributions to this spectroscopic signal. For the model employed, it is shown that the broad O–H stretching band is due to an overlap, and consequent mixing, of antisymmetric and symmetric stretching motions. These bands overlap because, in the condensed phase, they explore the anharmonic regions of the O–H stretching Morse potentials. Participation ratio results for the O–H region demonstrate that the center of the band represents 2–4 water molecules involved in each INM, while the red and blue wings of the band are primarily single or two molecule vibrations, suggesting that the O-H stretching motions are not especially collective. QINM methods are also applied to the water spectrum and are compared to INM methods. QINM spectra are derived from numerically exact path integral simulations and therefore produce the correct bond length distributions for intramolecular motions, and account for quantum dispersion effects associated with light atoms.

The remainder of the paper is arranged as follows: The molecular dynamics, path integral, and many body polarization methods are briefly summarized in Sec. II. The INM approximation to the DOS is derived in Sec. III, and then the INM DOS is used in evaluating the golden rule expression for IR absorption. Section IV compares theoretical and experimental intermolecular and bending IR spectrum of water. Section V does the same for the O–H stretching absorption. The paper is concluded in Sec. VI.

II. METHODS

Classical and path integral molecular dynamics (MD) simulations were performed using a code developed at the Center for Molecular Modeling at the University of Pennsylvania, which uses reversible integration and extended system techniques.[36,37] Microcanonical MD simulations were performed on water with an average temperature of 300 K and a density of 1.0 g/cm^3. In all cases the results were tested and found to be system size independent. Most results were generated from 64 molecule simulations, and different system sizes up to 512 molecules were tried. The path integral MD simulations were carried out with 8 and 16 pseudoparticles per atom ($P=8$ and $P=16$) and the results were converged with $P=8$.[38] TCF data collection was carried out over 200 picoseconds, with configurations saved every 0.5 femtoseconds. INM data collection was carried out over 100 picoseconds with instantaneous configurations stored every 200 femtoseconds. Thus, the computational effort in obtaining the TCF spectra (correlating 400 000 configurations including a matrix inversion at each step to solve the many body polarization equations) is far greater than that required for the INM spectra calculation (500–1000 configurations).

Simulations were employed using simple, flexible water models, primarily SPC-F modified with a Morse O–H stretching potential.[31] The O–H bond was modeled both as a Morse oscillator and harmonic oscillator, and the Morse potential produced the best approximation to the O–H stretching region of the IR spectrum. Both a harmonic and Morse oscillator representation of the bending potential were employed, and the results were comparable; the results below employ the harmonic bending potential.[31] A flexible TIP3P model[20] was also implemented, but did not significantly change any of the vibrational spectrum.

The potential and electrostatic parameters are summarized elsewhere.[20,31] Briefly, in performing the MD, within the SPC-F model, water electrostatics are represented by partial charges on the atoms, which are chosen to reproduce the average condensed phase water dipole moment.[20] In calculating the spectrum, partial charges are placed on the atoms and are chosen to reproduce the gas phase dipole moment, because polarization effects are explicitly included via a PAPA model.[39–41]

To model the polarizability of water, when calculating spectroscopic quantities, many body polarization equations are solved exactly by matrix inversion to calculate the induced dipoles and their derivatives as in our previous work.[9,10] Two sets of point polarizabilities were tried, and those used previously[32] ($\alpha_O=1.1482$ Å^3, $\alpha_H=0.3304$ Å^3) worked best. This choice of PAPA polarizabilities does lead to unphysically large induced dipoles and therefore a short range damping is introduced as was done in previous work.[32] The other set of PAPA polarizabilities treated only the oxygen as a polarizable center ($\alpha_O=1.43$ Å^3, $\alpha_H=0.0$ Å^3), and both sets of point polarizabilities give essentially the same molecular polarizability tensor.

The TCF approximation to the spectrum is solved in the standard fashion,[42] and the results are corrected to obey detailed balance as described along with the results. The charge contributions to the intramolecular vibrational line shapes are modified in the figures to account for the proper gas phase dipole derivatives as follows.[21,22] By choosing three partial charges to reproduce the gas phase permanent dipole, the dipole derivatives for the intramolecular motions are incorrect. Therefore the charge spectrum integrates to the dipole derivative that the point charge model produces, which is too large for the bending and stretching motions. Therefore, the charge spectra are divided by the ratio of the experimentally observed gas phase dipole moment to those which our partial charges give. The total signal is then modified to correct the cross term contribution to the spectrum, i.e., the part of the spectrum which originated from the cross correlation be-

tween the permanent and induced dipole moments.[32,43]

No modification is needed in the intermolecular spectral region because the permanent charge absorption spectrum is determined by the magnitude of the dipole itself. The induced contributions also do not need to be modified in any region of the spectrum. This scaling is just a computational convenience, and the proper dipole derivatives can be incorporated into a more complex model of the electrostatics. This can be accomplished easily within the INM method because projections of each INM onto the molecular normal modes are easily accomplished. This approximation does not significantly affect the O–H stretching results as the condensed phase absorption is dominated by the induced dipole contribution. When necessary, scaled regions are indicated in the figures by two vertical lines on the abscissa. Where appropriate, the figures display imaginary INM contributions on the negative abscissa.

The participation ratio is calculated as in our previous work.[44] The projected DOS and spectra are calculated as in previous work.[8,27] Briefly, each INM is projected onto the gas phase INMs for a given molecule, and all gas phase molecular contributions are summed over all the molecules for a specific mode type (translational, bending, and so on). A gas phase INM is calculated by taking the molecules geometry from the liquid and diagonalizing its force constant matrix in the absence of intermolecular interactions. Projected DOS and spectra (weighted DOS) are then constructed like their INM counterparts using the fractional projections onto gas phase modes as weighting factors.

III. THE INM AND QINM APPROXIMATION OF THE VIBRATIONAL DOS

The canonical vibrational DOS of a system can be written as the trace of a Hamiltonian matrix:[45]

$$\rho(E)=\mathrm{Tr}\{e^{-\beta H}\delta(H-E)\}/Z, \tag{3.1}$$

$$\rho(E)=\frac{1}{2\pi\hbar}\int dt\, e^{-iEt/\hbar}\mathrm{Tr}\{e^{-\beta H}e^{-itH/\hbar}\}/Z, \tag{3.2}$$

$$\rho(E)=\frac{1}{2\pi\hbar}\int dt\, e^{-iEt/\hbar}\mathrm{Tr}\{e^{-\lambda H}\}/Z, \tag{3.3}$$

$$\lambda=\beta-it/\hbar, \tag{3.4}$$

$$Z=\mathrm{Tr}\{e^{-\beta H}\}. \tag{3.5}$$

Above, H is the Born–Oppenheimer Hamiltonian, and $\beta=1/kT$. The DOS has the form of the Fourier transform of a partition function evaluated in complex time. In the energy representation, Eq. (3.3) takes the form

$$\rho(E)=\sum_i \exp(-\beta E_i)\,\delta(E-E_i)/\sum_i \exp(-\beta E_i). \tag{3.6}$$

Employing the isomorphism between a quantum mechanical (QM) path integral calculation and the statistical mechanical classical ring polymer system,[38,46–49] the complex time partition function in Eq. (3.3) can be written for a liquid of N atoms, each represented by P ''beads:''

$$Z_P^c=\left(\frac{mP}{2\pi\hbar^2\lambda}\right)^{3NP/2}\int d\mathbf{r}^1\cdots d\mathbf{r}^P \exp(-\lambda(\phi+V)), \tag{3.7}$$

$$\phi=\frac{mP}{2\lambda^2\hbar^2}\sum_{t=1}^{P}\sum_{j=1}^{N}(\mathbf{r}_j^{(t)}-\mathbf{r}_j^{(t+1)})^2, \tag{3.8}$$

$$V=\frac{1}{P}\sum_{t=1}^{P}\sum_{i>j}^{N}U(\mathbf{r}_i^{(t)};\mathbf{r}_j^{(t)}). \tag{3.9}$$

In Eqs. (3.7)–(3.9), Z_P^c is the discretized version of the complex time partition function, and $\mathbf{r}^{(t)}$ is a $3N$ dimensional vector of all the atom positions for a given t. Above, ϕ has its origin as the kinetic energy portion of the path integral, and V results from the potential energy contribution. U is the total potential energy function for the system, and is shown as a two body potential for convenience.

One can now proceed to Taylor expand V to second order for a given configuration, $\mathbf{r}_0$, and to introduce normal coordinates. Because the interpolymer interactions only involve beads that have the same value of t, the 3NP×3NP second derivative matrix of V is block diagonal. This allows the locally expanded potential to be written

$$V=V(\mathbf{r}_0)+\sum_{t=1}^{P}\sum_{i=1}^{N}\left(\frac{\partial V}{\partial r_i^t}\right)_{\mathbf{r}_0} r_i^t+\sum_{t=1}^{P}\sum_{i,j=1}^{N}\left(\frac{\partial^2 V}{\partial r_i^t r_j^t}\right)_{\mathbf{r}_0} r_i^t r_j^t. \tag{3.10}$$

The quadratic term in the potential expansion corresponds to the sum of P force constant matrices multiplying the coordinates. One can then introduce normal coordinates, $\mathbf{Q}^t=\mathbf{D}_t^T\mathbf{r}^t$, where $\mathbf{D}_t$ is a unitary transformation of the coordinates that diagonalizes the tth force constant matrix in Eq. (3.10). Under this coordinate transformation Eqs. (3.7)–(3.9) can be written as

$$Z_P^c=\left(\frac{mP}{2\pi\hbar^2\lambda}\right)^{3NP/2}\int d\mathbf{Q}^1\cdots d\mathbf{Q}^P \exp(-\lambda(\phi+V)), \tag{3.11}$$

$$\phi=\frac{mP}{2\lambda^2\hbar^2}\sum_{t=1}^{P}(\mathbf{Q}^{tT}\mathbf{Q}^t+\mathbf{Q}^{(t+1)T}\mathbf{Q}^{t+1}-2\mathbf{Q}^{tT}\mathbf{D}_t^T\mathbf{D}_{t+1}\mathbf{Q}^{t+1}), \tag{3.12}$$

$$V=\frac{1}{P}\sum_{t=1}^{P}\sum_{i}^{3N}\frac{\omega_i^{t2}}{2}Q_i^{t2}. \tag{3.13}$$

Above ω_i^{t2} is the ith eigenvalue of the tth force constant matrix. In the continuous limit ($\lim_{P\to\infty}$), Eqs. (3.11)–(3.13) become $3N$ separate path integrations for harmonic oscillators with a time dependent frequency. The time dependence of the frequency is a consequence of each ''bead'' exploring a different portion of the potential surface and consequently experiencing a different locally harmonic potential. Several approximations to Eqs. (3.11)–(3.13) are possible. As P gets sufficiently large, for a given system, $\mathbf{Q}^{tT}\mathbf{D}_t^T\mathbf{D}_{t+1}\mathbf{Q}^{t+1}$ approaches $\mathbf{Q}^{tT}\mathbf{Q}^{t+1}$, and in that limit the integrations can be carried out analytically,[45] resulting in an analytic approximation to Z_c, which can then be Fourier transformed to approximate the DOS; this approach is being pursued. Alterna-

tively, the continuous path integration for the time dependent harmonic oscillator can also be solved.[45] In this case, $\omega^2(t)$ can be approximated as a Gaussian random variable,[10] and appropriate solutions might be found.[45,50] The simplest approach, pursued here, is to neglect the quantum dispersion in the kinetic energy term (setting ϕ to zero), which results in a classical partition function for $3N$ P harmonic oscillators. These harmonic frequencies and coordinates are then used in approximating the absorption golden rule formula (described below) resulting in an approximation which will be referred to as the QINM method. The QINM approach takes account of the temperature dependence of vibrational amplitudes which classical mechanics cannot describe accurately.

If the potential energy of the system is harmonic, then the path integrations can be carried out exactly. The resulting DOS can be expressed for a given coordinate i:

$$\rho(E)=(1/Z)\int dt\, e^{-iEt/\hbar}e^{-\beta\hbar\omega_i/2}e^{i\omega_i t/2}e^{-\beta\overline{V}}e^{it\overline{V}/\hbar} \times\sum_{v=0}^{\infty} e^{vi\omega_i t}e^{-v\beta\hbar\omega_i}, \tag{3.14}$$

$$\rho(E)=(1/Z)e^{-\beta\overline{V}}\sum_{v=0}^{\infty} e^{-\beta(v+1/2)\hbar\omega_i} \times\delta\left(E-\left[\left(v+\frac{1}{2}\right)\hbar\omega_i+\overline{V}\right]\right), \tag{3.15}$$

$$\overline{V}=V(\mathbf{r}_0)+\sum_i (\mathbf{D}_t^T\mathbf{f})_i^2/(m\omega_i^2). \tag{3.16}$$

In Eq. (3.16), $\mathbf{f}$ is the vector of system forces for the reference configuration; $\overline{V}$ would vanish if the reference configuration is an extremum of V. The first potential derivative term in $\overline{V}$ causes a frequency shift of all states and does not affect the spectrum. The contribution to the DOS for a given mode and configuration is seen to be the thermally weighted harmonic oscillator energy spectrum.[45] This is the desired result because it associates the local second derivative of potential energy with the QM harmonic frequency, ω, which appears in the DOS.

As a consequence, it is reasonable to construct a QINM DOS from a path integral simulation by diagonalizing the P force constant matrices in Eq. (3.10), and creating a histogram of the frequencies that are obtained. Each force constant matrix is symmetric and only of size $3N\times 3N$. Thus, obtaining the QM DOS from a PIMC approach is reasonable from a computational point of view, i.e., each path integral configuration simply spawns P classical configurations. DOS constructed by this procedure will be referred to as QINM DOS. A QINM DOS is a quantum locally harmonic approximation to the actual DOS, and is exact for harmonic systems. If the system is behaving classically, each ''bead'' will experience the same harmonic potential ($\omega_i^{t2}=\omega_i^2$), and classical mechanical behavior is recovered in Eqs. (3.7)–(3.9). This is the standard INM approximation to the DOS. Consequently, the INM DOS can be described as classical locally harmonic approximation to the true DOS. The QINM DOS will then reflect the correct bond length distributions for the intramolecular vibrational modes. This would be expected to be important in modeling the intramolecular vibrations, and will also correctly describe the thermodynamic coupling between the rotations and vibrations. The QINM approach also correctly describes any tunneling or quantum dispersion contributions to the DOS which may be important for light atoms or low temperatures. It should be noted that vibrational DOS, or related quantities, have been calculated using PIMC and similar methods in a limited number of cases previously.[51–53] Another possible approximation is to take the centroids of the path integrals as a set of classical positions in evaluating the force constant matrix; this is currently being investigated.

Given an INM or QINM approximation to the vibrational DOS, one proceeds to evaluate the relevant golden rule expression. Considering infrared spectroscopy the Beer–Lambert absorption coefficient, $\alpha(\omega)$, multiplied by the frequency dependent index of refraction, $n(\omega)$, can be written[42]

$$n(\omega)\alpha(\omega)=\frac{\pi\omega}{\epsilon_0\hbar cV}(1-e^{-\beta\hbar\omega}) \times\sum_v\sum_w \rho_w|\mathcal{M}_{vw}|^2\delta(\omega-\omega_{vw}). \tag{3.17}$$

In Eq. (3.17), ϵ_0 is the permittivity of free space, c is the speed of light, V is the system volume, and $|\mathcal{M}_{vv'}|^2$ is the transition matrix element between vibrational states v and w.

Next, the dipole moment is Taylor expanded to first order and the matrix elements in Eq. (3.17) are evaluated for harmonic oscillators to give

$$\langle n(\omega)\alpha(\omega)\rangle=\frac{\pi}{6c\epsilon_0}\left\langle\left[\left(\frac{\partial\mu_x}{\partial Q_k}\right)^2+\left(\frac{\partial\mu_y}{\partial Q_k}\right)^2 +\left(\frac{\partial\mu_z}{\partial Q_k}\right)^2\right]\delta(\omega-\omega_k)\right\rangle. \tag{3.18}$$

The angle brackets represent averaging over a thermal distribution of liquid configurations, $\boldsymbol{\mu}$ is the system dipole vector and the contribution of INM Q_k is being considered. The delta function (the vibrational DOS) is then replaced by its INM or QINM approximation to arrive at the weighted DOS approximation to the IR spectrum. This same procedure can be repeated for Raman or other spectroscopies.[11,13,15] Also, more complex models of the dipole or polarizability function can be incorporated.[15,54] Approximating the spectrum in this fashion naturally accounts for detailed balance[28,33,34] because we are treating a liquid as an effective ensemble of harmonic solids, and this is an attractive feature of INM approaches which will be discussed below.

One problem that arises within INM and QINM approaches is the presence of regions of negative curvature in the potential surface and resultant imaginary modes. In modeling spectroscopy it has been suggested by ourselves[9,10] and others[14] that imaginary INMs contribute like real INMs at the magnitude of their imaginary frequency. This simple approximation works quite well, and will be adopted in this paper, but it is still desirable to do better. One approach is to set $P=1$ in Eqs. (3.7)–(3.9) and then to do the resulting time integral in Eq. (3.3), leaving one with an expression for the

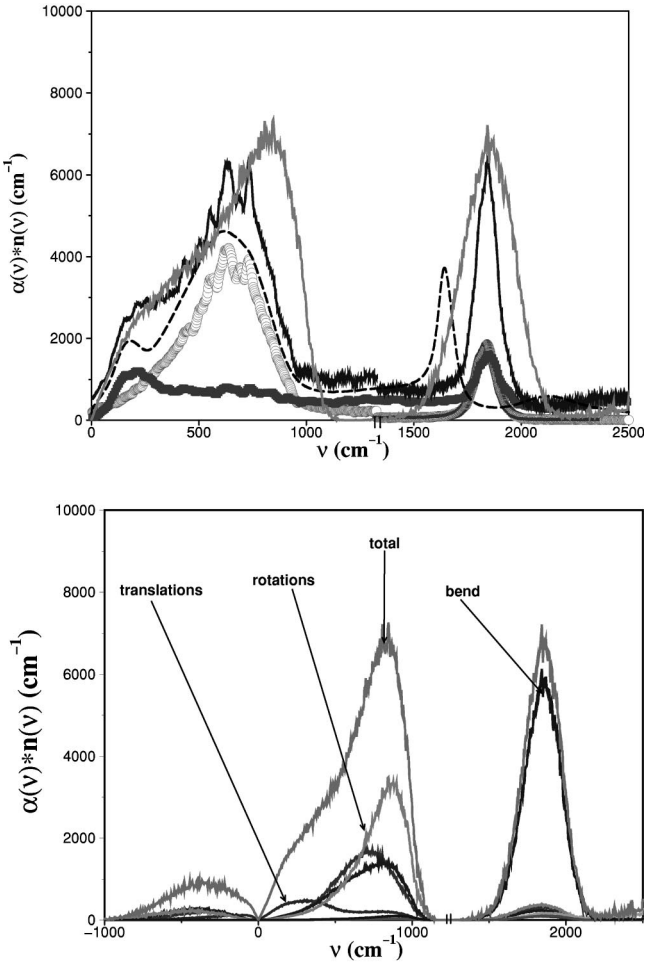

FIG. 1. (a) Experimental and theoretical results (INM and TCF) for the intermolecular and bending IR spectrum are presented. The experimental result is the dashed line, while the INM result is the jagged line which gives the broader bending spectrum. Imaginary INMs are contributing to the spectrum at the magnitude of their imaginary frequencies, and make only a small contribution. The jagged line represents the TCF result. Also shown is the TCF result calculated using only the induced dipole contribution (smallest magnitude line with solid squares) and the TCF result using only the permanent charge contribution (open circles). (b) The theoretical result for the INM spectra (the weighted DOS) is shown with the imaginary frequencies represented on the negative frequency axis (the uppermost jagged line labeled total). The INM spectrum is broken up into projections onto the molecular gas phase INMs, and the linetypes are labeled. Note that three distinct rotational projections are shown, and the rotational contributions were distinguished by coordinated transformation into the principal axis frame. The three translational contributions are indistinguishable.

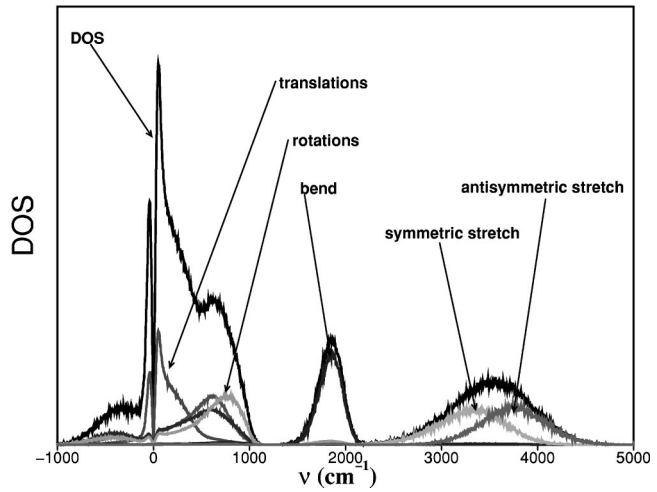

FIG. 2. The (unweighted) DOS and its molecular components. The INM DOS is broken up into its projections onto the molecular gas phase INMs, and the linetypes are labeled.

classical DOS. This might be evaluated, perhaps for a simple model such as a one dimensional double well or Morse potential, in order to assess how the regions of negative curvature contribute. This approach is the subject of ongoing investigation.

IV. THE INTERMOLECULAR AND BENDING IR SPECTRUM

The intermolecular spectroscopy of water has been carefully modeled using molecular dynamics methods previously.[32,43] Figure 1(a) presents the intermolecular spectrum of water as calculated by both the INM and TCF approaches, and contrasts these results with the experimental spectrum [the product of individually measured $n(\nu)\alpha(\nu)$] due to Bertie.[21,22,30] Overall agreement between TCF and experiment is excellent as has been noted previously.[32,43] The INM approximation is excellent from zero to 500 cm^{-1}. Up to 200 cm^{-1}, including the imaginary modes results in improved agreement with experiment. This is consistent with the success of INM approximations to other intermolecular spectra in molecular liquids,[9,10,13] and intermolecular spectra in those cases do no extend past a few hundred wave numbers. From about 200–500 cm^{-1} the real INM signal is in somewhat better agreement (this can be seen in the figure comparing the INM and QINM results below), and the nature and contribution of the high frequency imaginary modes merits investigation. At higher frequencies, 500–1000 cm^{-1}, the INM spectrum is somewhat too large, although the falloff around 1000 cm^{-1} is reasonable. The disagreement in this region results from an overestimation of the induced contribution to the INM spectrum relative to its contribution to the TCF spectrum. The reason for this is unclear.

The INM method offers information complimentary to the TCF results. Figure 1(b) shows the projected INM spectra which breaks the full spectrum into its molecular modal contributions, i.e., into the amount that each molecules translational, rotational and individual vibrational mode contribute. The DOS itself was similarly analyzed in an earlier paper[27] for frequencies below water bending; the model employed in that work was rigid. The spectral breakdown is somewhat different than the (unweighted) density of states, as would be expected for a frequency dependent weighting factor. The projected and total DOS are presented in Fig. 2, and one can see distinct differences in the absorption (weighted DOS above), notably the enhancement of the rotational absorption in the actual spectrum. The hindered translational contribution is clearly non-negligible, and weighting the DOS enhances this feature.

The agreement between the TCF and experimental results is perhaps less robust than one might assume. The classical time correlation function results do not obey detailed balance and a symmetrization procedure must be

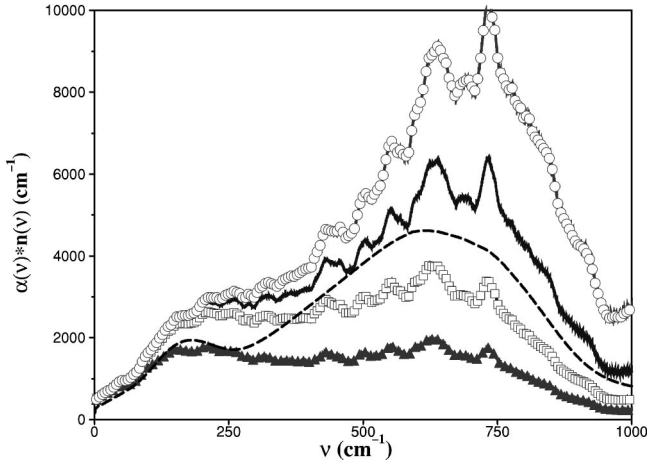

FIG. 3. The influence of detailed balance correction on the classical TCF is demonstrated. The lower line with solid triangles represents the uncorrected TCF result. The open squares represent the $2/(1+e^{-\beta\hbar\omega})$ correction factor, while the $\beta\hbar\omega/(1-e^{-\beta\hbar\omega})$ corrected TCF is the solid jagged line. The $e^{\beta\hbar\omega/2}$ correction is the line with open circles. Also shown is the experimental spectrum (dashed line) for comparison.

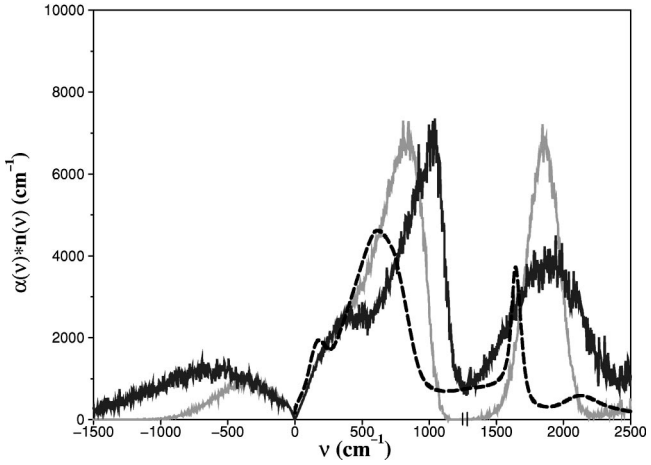

FIG. 4. Experimental and theoretical results (INM and QINM) for the IR spectrum are presented. The INM result is the jagged line, while the QINM result is the jagged line. Imaginary INM and QINM contributions are shown on the negative abscissa. The experimental data is the dashed line.

adopted.[33–35] Alternatively, one can directly approximate the symmetrized quantum TCF with the classical correlation function, but this amounts to choosing a certain detailed balance correction to the desymmetrized classical TCF, i.e., multiplying by $2/(1+e^{-\beta\hbar\omega})$. This factor is not the only possible choice,[33] and we compare a few common choices in Fig. 3. The figure displays the intermolecular spectrum when the following frequency domain detailed balance factors are employed:[33] $2/(1+e^{-\beta\hbar\omega})$, $\beta\hbar\omega/(1-e^{-\beta\hbar\omega})$, and $e^{\beta\hbar\omega/2}$. The TCF results are also shown uncorrected, and the experimental curve is also shown for comparison. These detailed balance factors vary dramatically in their high frequency behavior, from a constant factor to linear and exponential growth, respectively. One can see this selection has a dramatic effect on the results. This is especially important for the unusually broad water intermolecular spectrum. In fact, unlike many molecular liquids, water has no spectral window in the infrared. One advantage of the INM methods is that detailed balance is built in because the liquid is described as an effective set of harmonic oscillators. This makes the INM approach more stable in that sense. This will be especially important when we quantitatively treat high frequency vibrations below. It is worth noting that the $\beta\hbar\omega/(1-e^{-\beta\hbar\omega})$ correction works best here (and at higher frequencies as will be demonstrated below), and also leads to excellent agreement with experiment in CS_2[10] and CO_2.[55]

Figure 4 contrasts the QINM, INM, and experimental results. The classical INM results do not do a good job in modeling the region of the spectrum above 1000 $cm^{-}1$ and below the bending feature. The QINM methods seem to capture the absence of a spectral window throughout the spectrum (this is perhaps not surprising in that the QINM methods correctly treat thermodynamic couplings between rotational and translational motions). The TCF results can show the presence or absence of a window depending on the detailed balance factor that is used, and the $\beta\hbar\omega/(1-e^{-\beta\hbar\omega})$ factor works best in this region as well. It is clear from the figure that the INM and QINM methods do become coincident at low frequencies ($\hbar\omega \ll k_B T$).

The origin of the 200 cm^{-1} feature in the spectrum has been the subject of some interest.[26,32] Figure 1(a) shows a bump due to many body polarization effects, and it is more easily seen in the induced contribution than the full spectrum. To confirm the origin of this feature we performed simulations with larger effective charges on the water molecules and the feature becomes far more prominent. Also, only with the inclusion of collective many body polarization effects does a feature appear at all,[32] and any such feature was absent in single molecule TCF results, i.e., when the TCF is constructed without cross terms in the dipole moment product. The projected INM weighted spectra suggest this feature is the result of a combination of rotational and hindered translational motions, although it is not possible to assume an exact correspondence between the INM and experimental frequency. The overly broad INM spectra can be thought of as resulting from lack of inclusion of motional narrowing effects on the spectrum. Interestingly, although the INM spectra display a window between the intermolecular and bending spectrum, some bending character is present in the high frequency wing of the intermolecular spectrum, indicated some coupling even in the classical result. This observation was confirmed by animating INM motions from the region, and observing modes which were clearly bendlike in character.

The origin of the main feature 680 cm^{-1} is due primarily to permanent dipoles, and clearly results from hindered rotational (librational) motions; projection onto the molecular translations is negligible at higher frequencies, and the induced effects favor hindered translations over rotations.

The TCF bending line shape [Fig. 1(a)] is very similar to that seen experimentally and the intensity is somewhat too large. This is a result of the polarization contribution which is not negligible in our model, but is found to be insignificant experimentally.[21,22] The bending spectrum that results from the charge contribution alone is in excellent agreement with experiment in shape and magnitude. The central frequency is

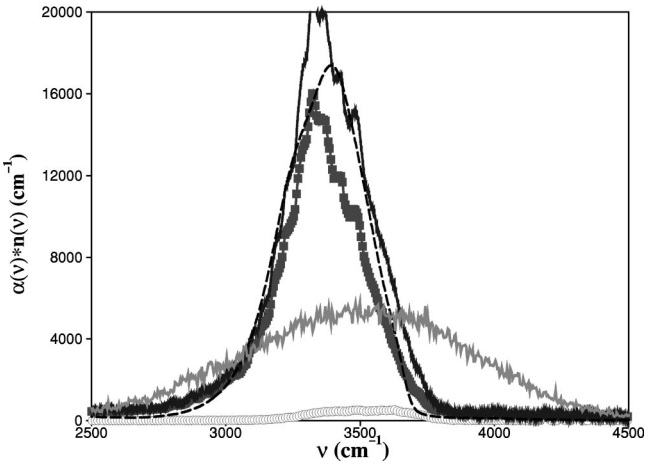

FIG. 5. Experimental and theoretical (induced INM and TCF) results for the O–H stretching region of the IR spectrum is presented. The dashed line is the the experimental data. The INM result is the jagged line. The TCF result (jagged line) is shown with its permanent charge (open circles) and polarizability induced (solid squares) contributions.

blueshifted by about 100 cm^{-1}, and is due to a deficiency in the model potential. Better intramolecular potentials exist,[12] and are currently being tested.

V. THE O–H STRETCHING IR SPECTRUM

Figure 5 compares the experimental O–H stretching spectrum with the spectrum calculated by TCF and INM methods. The agreement between the TCF and experimental spectrum is striking. The harmonic frequencies (at the minimum of the Morse potential) for the SPC-F model are $\nu_1=3841$ cm^{-1} and $\nu_3=3966$ cm^{-1}.[31] These frequencies were intended to match the gas phase frequencies but are about 5% too high. In the condensed phase the intermolecular interactions cause the molecules to explore the anharmonic regions of the potential surface, and this lowers the bands central frequency by a few hundred wave numbers. In the model used here, the anharmonicity is incorporated through a Morse O–H stretching potential.[31] Also, as a result of the frequency redshift, the symmetric (ν_1) and antisymmetric (ν_3) motions mix strongly and form the single broad absorption shown in the figure.

Typically, condensed phase absorptions integrate to the value of the gas phase squared dipole derivative. This is the case with the water bending absorption, and this usually indicates that polarization effects are unimportant. In contrast, the water O–H stretching absorption grows a factor of 19 from the gas to liquid phase.[21,22] In our model, the polarization effects are represented by way of a PAPA model. PAPA models the polarizability of the system by placing point polarizabilities on the atoms which reproduce the molecules polarizability tensor. In the condensed phase, dipoles are induced in molecules by the electrostatic field of the surrounding molecules. Induced dipoles interacting with each other are handled by solving many body polarization equations.

Induced effects contribute along with a permanent charge contribution from the motion of the partial charges on the atoms. The partial charges on the atoms are chosen to reproduce the gas phase dipole for the purpose of calculating the spectra. This is in contrast to the charges which are used in the dynamics, which are chosen to reproduce the average condensed phase dipole moment. This model of the system dipole nearly quantitatively reproduces both the O–H absorption line shape and its integrated intensity. It is interesting that the charge absorption spectrum is blueshifted to the induced contribution and this creates a slight asymmetry in the line shape. It is surprising that a simple classical water model, supplemented with a PAPA polarizability model for the purpose of calculating the spectrum, can describe this feature so accurately.

This agreement does depend on the choice of detailed balance factor, and the $\beta\hbar\omega/(1-e^{-\beta\hbar\omega})$ quantum correction factor is used. This correction factor brings the classical harmonic oscillator absorption spectrum into agreement with the QM spectrum.[9] The line shape itself is not greatly affected by the choice of correction factor, but the magnitude of the band is quite different for different choices. This harmonic correction factor seems to be the most reasonable for several reasons. The factor achieved the best agreement with experiment in our previous investigations in CS_2 and CO_2. When treating stretching motions, the harmonic oscillator correction is an obvious choice. Also, the integrated intensity of the (broader) charge and induced INM line shapes are the same as the TCF result which is corrected with the harmonic oscillator factor.

It is notable that the INM spectra shift to nearly the same central frequencies as their time correlation function counterparts. Further, their components integrate to about the same charge and induced absorption. These observations are supportive of a motional narrowing interpretation of the INM results.

To test the importance of the PAPA model employed, two different models were evaluated. The results shown are from a model with point polarizabilities on each atom. The other model placed polarizability only on the oxygen. This model gave similar results for all the spectrum except for the O–H stretching region. The O–H stretching line shape was about the same, but the induced intensity was significantly diminished. Although both models give similar molecular polarizability tensors, the distributed model is physically more reasonable.[32] The location of polarizable centers on the hydrogen atoms is apparently very important in capturing the large induced collective O–H absorption in the liquid. This may not be surprising given the close proximity of of hydrogen and oxygen in hydrogen bonds that results in coupling between the charge distributions during the O–H stretching motion.

The question of why a classical model should be so effective is a difficult one. The complex, high frequency, O–H absorption would be expected to require a quantum mechanical treatment because the vibrational modes are ground state dominated oscillators.[12] When treating harmonic oscillators, a classical description of spectroscopy can be effective.[9,28] However, the O–H stretching potential is highly anharmonic and the anharmonicities dramatically influence the spectrum. One possibility is that each absorbing mode is exploring only a small region of the anharmonic potential surface as a result

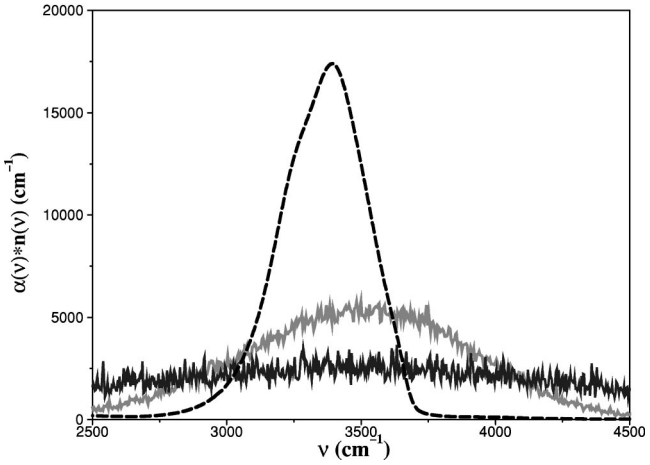

FIG. 6. The theoretical, induced INM and QINM, results for the O–H stretching region of the IR spectrum. The upper, jagged line is the INM result, while the lower, jagged line is the QINM result. Also shown is the experimental spectrum (dashed line) for comparison.

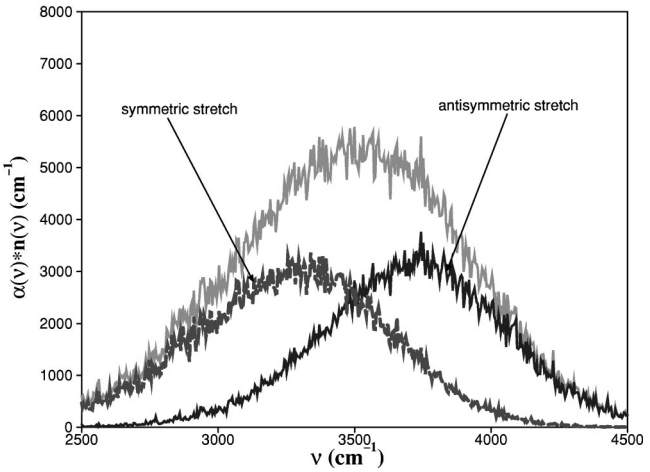

FIG. 7. The induced INM result for the O–H stretching region of the IR spectrum is broken down into its modal contributions. The uppermost, jagged line is the INM result, while the lower left contribution is the symmetric stretching contribution and the lower right is the antisymmetric stretching contribution.

of each molecule's local liquid environment. Around the region of the potential surface that the mode is residing, the potential may be nearly locally harmonic, and the broad band width would then be due to inhomogeneous broadening, brought about by differing local environments. The absorbing modes would then be effectively harmonic coordinates, which have the same absorption properties both classically and quantum mechanically. Some support for this hypothesis comes from the observation that the center of the liquid O–H band is far removed from with the gas phase ν_1 and ν_3 frequencies. This suggests that in the liquid the molecules are substantially distorted and the minimum of the gas phase potential is less frequently visited.

Figure 6 contrasts the INM, QINM, and experimental spectra. The QINM spectrum has the same central frequency but is significantly broader. The QINM spectrum (induced and charge) integrates to the same absorption over the entire band. Unfortunately the total signal (the squared sum of the charge and induced contribution) for the QINM and INM methods is less than the sum of the individual signals, implying that the cross term in the squared sum is negative for the INM and QINM methods. This is in contrast to the TCF and experimental cases. Interestingly, the TCF, INM, and QINM spectra were all additive in the intermolecular region. Overall, the INM results seem superior to the QINM results, although the QINM results are not unreasonable. The QINM method is essentially a mixed quantum classical approximation, and treating systems on an entirely classical footing is often superior to a mixed description.[28]

Given a model which accurately describes the O–H stretching absorption line shape, INM methods can be employed to analyze the molecular origin of the signal. Within the motional narrowing picture the INMs with frequencies to the blue or red side of the band center are associated with absorption on the same side of the band. Figure 7 displays the projection of the induced INM signal onto the different molecular motions, and the induced contribution represents 95% of the total signal. This is contrasted with the total induced INM signal, and the experimental absorption is shown for reference. These results suggest that the origin of the broad absorption is the mixing of symmetric and antisymmetric stretching motions due to the overlap in their frequencies, which itself is a consequence of the large anharmonicity and inhomogeneous broadening of both stretches. It is clear that both motions contribute roughly half the total intensity, and predominantly through the induced absorption mechanism. In contrast, in the gas phase the symmetric stretching motion is about 20 times more intense in its absorption compared to the antisymmetric stretching absorption.

To demonstrate this conclusion, Fig. 8 shows molecular snapshots with a typical INM, animated with arrows, representing the INM motion. The first INM was taken from the far blue portion of the band and is antisymmetric stretching in character and not particularly collective. The second INM is taken from the far red of the band and exhibits symmetric stretching character, and also involves only a small number of molecules. The third INM is taken from the center of the band, and the motion is characteristic of a linear combination of symmetric and antisymmetric motions, which results in most of the motion involving only hydrogen on a given molecule.[56] The modes near the center of the band are slightly more collective then those further from the center. The modes from the center of the band often have one molecule each predominantly symmetric and antisymmetric stretching, respectively. Even then, one hydrogen is displaced much more than the other, which implies an unequally weighted linear combination of the motions. The modes toward the edge of the band rarely involve more than the motion of one molecule to any significant degree. These modes shown in Fig. 8 were typical and representative of the different band regions. The O–H stretching motions do involve more oxygen motion than the equilibrium gas phase normal mode motions,[56] which were animated for comparison, but are not shown here. This is possible in the condensed phase because the only constraint is that the center of mass of the entire system is not changed by an INM motion.

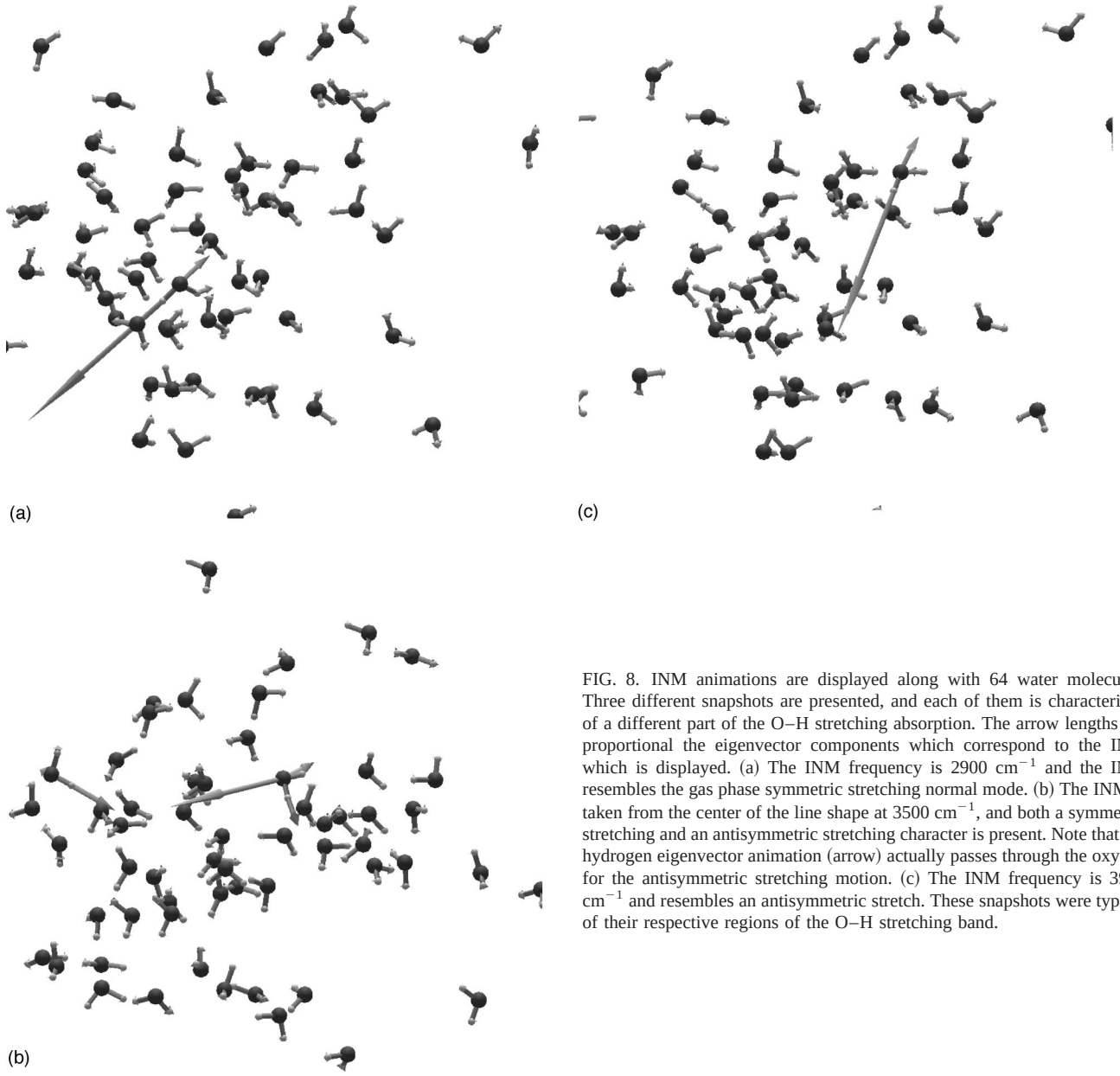

FIG. 8. INM animations are displayed along with 64 water molecules. Three different snapshots are presented, and each of them is characteristic of a different part of the O–H stretching absorption. The arrow lengths are proportional the eigenvector components which correspond to the INM which is displayed. (a) The INM frequency is 2900 cm^{-1} and the INM resembles the gas phase symmetric stretching normal mode. (b) The INM is taken from the center of the line shape at 3500 cm^{-1}, and both a symmetric stretching and an antisymmetric stretching character is present. Note that the hydrogen eigenvector animation (arrow) actually passes through the oxygen for the antisymmetric stretching motion. (c) The INM frequency is 3930 cm^{-1} and resembles an antisymmetric stretch. These snapshots were typical of their respective regions of the O–H stretching band.

Figure 9 quantitatively demonstrates the collective nature of the modes through the inverse participation ratio.[27,44] The results imply that the modes at the center of the band are only slightly more delocalized than those on the wings, and that all the stretching modes are more local than the rest of the spectrum. Further, it is found that in our model, which is clearly capable of describing the band shape in detail, the mode delocalization is fairly symmetric about the band center. It has been suggested that broadening occurs because the modes to the blue are localized and those to the red are more collective. However, our results suggest an alternative explanation for the broad O–H absorption: strong mode mixing between inhomogeneously broadened symmetric and antisymmetric stretching bands.

VI. CONCLUSION

INM spectroscopic methods used in conjunction with traditional TCF methods form a powerful tool for modeling and understanding condensed phase spectroscopy. Molecular dynamics together with classical TCF methods can describe complicated vibrational spectra, even with relatively simple models. Further, by comparing the resulting spectra with experiment, one can assess the adequacy of the assumptions that are inherent in the molecular model, and thus reduce the phenomenology to its essential components. For example, the present results imply that polarization effects need not be included explicitly in the molecular dynamics of water to reproduce its spectroscopy, and that simple molecular dynamics potentials can be very successful. Further, INM methods can be employed in a fashion complementary to TCF methods to ascertain the molecular origin of a spectroscopic signal.

It is becoming apparent that INM approximations to spectroscopy can often reproduce TCF (and experimental) results in the intermolecular region in relatively dense molecular liquids, where rotational motions are hindered.[9,10,13]

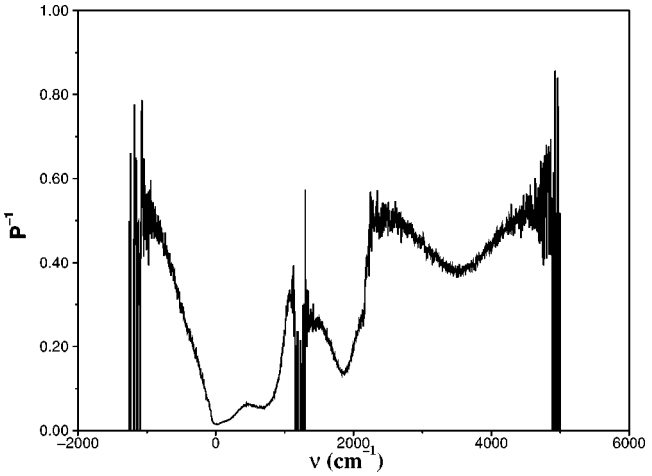

FIG. 9. The inverse participation ratio indicates the degree of localization of an INM. The inverse participation ratios was calculated as $P^{-1}(\omega_j) = \Sigma_{i=1}^{3N}(D_{ij})^4/(\Sigma_{i=1}^{3N}D_{ij}^2)^2$. P takes on the value of $1/3N$ for a totally delocalized mode and unity for a mode localized on one atom, where N is the number of atoms in the system.

In describing intramolecular motions, and intermolecular motions which involve relatively free rotation, INM methods produce spectral line shapes which are overly broad.[9,11] In water, the O–H stretching band center is redshifted hundreds of wave numbers from the gas phase vibrational frequencies.[31,12] By using Morse potentials to describe the O–H bonding potential this phenomena can be reproduced by both TCF and INM methods. These observations are all consistent with a motional narrowing interpretation of INM spectroscopy.[9,10] Also, INM derived spectra naturally account for detailed balance, while the choice of detailed balance factors to correct TCF results significantly influence the resulting spectra. Employing both TCF and INM methods together helps to resolve this difficulty.

Classical mechanical methods seem capable of describing phenomena that might be expected to only yield to a quantum mechanical analysis. By adding some quantum mechanics to the INM model in our QINM method, we arguably make the results worse. This is further evidence that purely classical mechanical models can be superior to mixing classical and quantum treatments.[28] Finally, we have proposed an explanation for the origin of the broad O–H stretching absorption in water, the band is a result of strong mixing of symmetric and antisymmetric stretching motions involving only a small number of molecules.

ACKNOWLEDGMENTS

The authors thank Jeffry Madura for numerous insightful comments and helpful conversations. Two of us (Brian Space and Preston B. Moore) thank Professor M.L. Klein for continuing encouragement in their collaboration. The research at Duquesne University was supported by an NSF Career Grant (No. CHE-9732945) to Brian Space. This research was supported in part by Grant No. CHE960007P from the Pittsburgh Supercomputing Center. The authors also thank the Space Foundation for partial support. Heather Ahlborn gratefully acknowledges support from the Bayer Research Fellowship.

[1] T. Keyes, J. Phys. Chem. **101**, 2921 (1997).
[2] R. M. Stratt, Acc. Chem. Res. **28**, 201 (1995).
[3] J. Adams and R. Stratt, J. Chem. Phys. **93**, 1632 (1990).
[4] B. Ladanyi and R. Stratt, J. Phys. Chem. **99**, 2502 (1995).
[5] T. Keyes, J. Chem. Phys. **104**, 9349 (1996).
[6] P. Moore and T. Keyes, J. Chem. Phys. **100**, 6709 (1994).
[7] P. Moore, A. Tokmakoff, T. Keyes, and M. Fayer, J. Chem. Phys. **103**, 3325 (1995).
[8] B. Space, H. Rabitz, A. Lőrincz, and P. Moore, J. Chem. Phys. **105**, 9515 (1996).
[9] P. Moore and B. Space, J. Chem. Phys. **107**, 5635 (1997).
[10] P. B. Moore, X. Ji, H. Ahlborn, and B. Space, Chem. Phys. Lett. **296**, 259 (1998).
[11] T. Keyes, J. Chem. Phys. **106**, 46 (1997).
[12] J. R. Reimers and R. O. Watts, Chem. Phys. **91**, 201 (1984).
[13] M. C. C. Ribeiro, M. Wilson, and P. Madden, J. Chem. Phys. **110**, 4803 (1999).
[14] J. T. Kindt and C. A. Schmuttenmaer, J. Chem. Phys. **106**, 4389 (1997).
[15] R. L. Murry, J. T. Fourkas, and T. Keyes, J. Chem. Phys. **109**, 2814 (1999).
[16] R. B. Williams and R. F. Loring, J. Chem. Phys. **110**, 10899 (1999).
[17] S. Sastry, H. E. Stanley, and F. Sciortino, J. Chem. Phys. **100**, 5361 (1993).
[18] T. Kalbfleisch and T. Keyes, J. Chem. Phys. **108**, 7375 (1998).
[19] R. Kubo, in *Fluctuation, Relaxation and Resonance in Magnetic Systems*, edited by D. T. Haar (Oliver and Boyd, Edinburgh and London, 1961).
[20] S.-B. Zhu, S. Singh, and G. W. Robinson, *Water in Biology, Chemistry and Physics* (World Scientific, New Jersey, 1996), see the refrences within.
[21] J. E. Bertie and H. H. Eysel, Appl. Spectrosc. **39**, 392 (1985).
[22] J. E. Bertie and Z. Lan, Appl. Spectrosc. **50**, 1047 (1996).
[23] P. Madden and R. W. Impey, Chem. Phys. Lett. **123**, 502 (1986).
[24] A. Wallqvist and O. Teleman, Mol. Phys. **74**, 515 (1991).
[25] P. Ahlström, A. Wallqvist, S. Engström, and B. Jönssom, Mol. Phys. **68**, 563 (1989).
[26] B. D. Bursulaya and H. J. Kim, J. Chem. Phys. **109**, 4911 (1998).
[27] M. Cho *et al.*, J. Chem. Phys. **100**, 6672 (1994).
[28] J. S. Bader and B. J. Berne, J. Chem. Phys. **100**, 8359 (1994).
[29] A. Wallqvist and B. J. Berne, Chem. Phys. Lett. **117**, 214 (1985).
[30] J. E. Bertie, the spectroscopic data is available in a convenient format at www.ualberta.ca/ jbertie/jebhome.htm
[31] K. Toukan and A. Rahman, Phys. Rev. B **31**, 2643 (1985).
[32] M. Souaille and J. C. Smith, Mol. Phys. **87**, 1333 (1996).
[33] J. Borysow, M. Moraldi, and L. Frommhold, Mol. Phys. **56**, 913 (1985).
[34] B. J. Berne, J. Jortner, and R. Gordon, J. Chem. Phys. **47**, 1600 (1967).
[35] S. Egorov and B. J. Berne, J. Chem. Phys. **107**, 6050 (1997).
[36] P. Moore and M. Klein (unpublished).
[37] M. Tuckerman, B. J. Berne, and G. J. Martyna, J. Chem. Phys. **97**, 1990 (1992).
[38] B. J. Berne and D. Thirumalai, Annu. Rev. Phys. Chem. **37**, 401 (1986).
[39] K. A. Bode and J. Applequist, J. Phys. Chem. **100**, 17820 (1996).
[40] J. Applequist, J. R. Carl, and K.-K. Fung, J. Am. Chem. Soc. **94**, 2952 (1972).
[41] J. Applequist and C. O. Quicksall, J. Chem. Phys. **66**, 3455 (1977).
[42] D. A. McQuarrie, *Statistical Mechanics* (Harper and Row, New York, 1976).
[43] B. Guillot, J. Chem. Phys. **95**, 1543 (1991).
[44] B. Space, H. Rabitz, and A. Askar, J. Chem. Phys. **99**, 9070 (1993).
[45] L. Schulman, *Techniques and Applications of Path Integration* (Wiley, New York, 1981).
[46] D. Chandler and P. Wolynes, J. Chem. Phys. **74**, 4078 (1981).
[47] K. S. Schweizer, R. M. Stratt, D. Chandler, and P. Wolynes, J. Chem. Phys. **75**, 1347 (1981).
[48] D. Thirumalai, R. W. Hall, and B. J. Berne, J. Chem. Phys. **81**, 2523 (1984).
[49] M. Herman, E. Bruskin, and B. J. Berne, J. Chem. Phys. **76**, 5150 (1982).
[50] W. Dittrich and M. Reuter, *Classical and Quantum Dynamics: From*

Classical Paths to Path Integrals (Springer, New York, 1996).
[51] G. Voth, Adv. Chem. Phys. **93**, 135 (1996).
[52] C. Chakravarty and R. Ramaswamy, J. Chem. Phys. **106**, 5564 (1997).
[53] S. Corcelli and J. Doll, Chem. Phys. Lett. **263**, 671 (1996).
[54] R. E. Larsen and R. M. Stratt, J. Chem. Phys. **110**, 1036 (1999).
[55] P. Moore, H. Ahlborn, and B. Space (unpublished).
[56] G. Herzberg, *Infrared and Raman Spectra of Polyatomic Molecules* (Van Nostrand, New York, 1946), p. 171.